SEMARAK ILMU PUBLISHING

Journal of Advanced Research in Numerical Heat Transfer

Journal homepage:
https://semarakilmu.com.my/journals/index.php/arnht/index
ISSN: 2735-0142

# Impact of Biomass Fuel Feeding Ratio in Co-firing Circulating Fluidized Bed Boiler: A Computational Fluid Dynamics Study

Sorathan Tanprasert[1], Nuttima Rangton[2], Warunee Nukkhong[2], Pitakchon Wises[2], Pornpote Piumsomboon[1], Benjapon Chalermsinsuwan[1,*]

[1] Department of Chemical Technology, Faculty of Science, Chulalongkorn University, 254 Phayathai Road, Wangmai, Pathumwan, Bangkok 10330, Thailand
[2] Integrated Research Center Company Limited, 122 Moo 2 Si Maha Phot, Prachinburi 25140, Thailand

**ARTICLE INFO**

***Article history:***
Received 13 November 2023
Received in revised form 14 December 2023
Accepted 16 January 2024
Available online 29 February 2024

***Keywords:***
Circulating fluidized bed; Computational fluid dynamics; Co-firing combustion; Gas emissions; Boiler efficiency

**ABSTRACT**

Nowadays, our global population is on a notable rise, coupled with an annual surge in energy consumption. The prevailing reliance on fossil fuels, especially in electricity generation, has significantly contributed to environmental pollution and exacerbated global warming. The circulating fluidized bed, distinguished for its continuous operation and effective heat transfer in the combustion chamber, emerges as a prominent boiler type. Furthermore, the use of biomass fuel, recognized for its renewable and environmentally friendly characteristics, presents an attractive option. Hence, exploring a co-firing system incorporating both coal and biomass as fuel feeds for the boiler holds promise, necessitating optimization for efficient energy production and reduced gas emissions. This study employs computational fluid dynamics to simulate the intricate interactions of solid fuel and flue gas reactions within the boiler, utilizing the two-fluid method for multiphase flow simulation. The circulating fluidized bed boiler in focus employs subbituminous coal, woodchips as biomass sources, and sand as the bed material. Model validation against operational data, including bed temperature, flue gas velocity outlet, and carbon dioxide mass fraction, indicates minimal deviation. Examination of the biomass ratio's impact on fuel feed reveals a reduction in sulfur dioxide emissions with an increasing biomass ratio, attributed to the lower sulfur content in woodchips compared to coal. However, a heightened woodchip blending ratio results in diminished boiler efficiency due to the altered heating value of the mixed solid fuel. The optimized biomass-to-coal ratio in fuel feeding is determined as 59.15%, achieving a maximized boiler efficiency of 82.84% and minimized pollution gas emissions of sulfur oxide and nitrogen oxide in accordance with industrial standards.

## 1. Introduction

Nowadays, there is a substantial increase in the global population, accompanied by a noticeable upward trend in energy consumption. According to a report covering energy consumption between 2000 and 2021 [1], there has been an approximate 49 percent rise in energy consumption.

* *Corresponding author.*
*E-mail address: benjapon.c@chula.ac.th (Benjapon Chalermsinsuwan)*

https://doi.org/10.37934/arnht.17.1.4454

Consequently, the emissions of gases produced from energy production processes are increasing dramatically. The primary sources of energy are fossil fuels and renewable energy sources. Electricity is a crucial source of energy for humankind, and various processes are involved in its production. One such process is the boiler, a conventional method that includes the thermal conversion of fuel to produce flue gas containing energy. This energy is then exchanged with water in a heat exchanger to generate steam. Finally, the steam is fed into a steam turbine for electrical production in the generator.

There are two main types of conventional boilers: fixed beds and fluidized beds. In this study, a fluidized bed boiler was chosen due to its continuous operation and its superior heat and mass transfer compared to a fixed bed boiler. However, there are drawbacks to this technology; erosion likely occurs in the reactor due to the motion of solids [2]. Regarding fuel feeding, two common types of fuel are used: coal and biomass. Due to global warming and the serious air pollution problems worldwide, emissions causing air pollution, such as sulfur dioxide resulting from the oxidation reaction due to sulfur content in coal fuel, must be managed. To address this, biomass is added to the fuel feed to reduce emissions. However, during the design phase, careful consideration must be given to the heating value of the fuel after combustion to maintain boiler efficiency, as investigated in several studies [3-5]. Additionally, the nature of biomass fuel, such as woodchips, includes a lower content of carbon and sulfur compared to coal [6]. This reduction in carbon and sulfur content contributes to a lesser impact on the environmental scope when biomass is used in combustion processes. The fuel feeding ratio of coal and biomass was conducted in Kim *et al.*, [7] They found that when the ratio of biomass increased in the fuel feeding of a laminar flow reactor, the amount of carbon monoxide increased along the tube due to volatile combustion. The trend of unburned carbon (%UBC) decreased due to the volatile component being higher in the large ratio of biomass to coal feeding. Consequently, the char combustion, which produces carbon monoxide, was influenced. Xie *et al.*, [4] found that as municipal solid waste (MSW) increased, the concentration of nitrogen oxide increased, but the concentration of sulfur dioxide decreased. Moreover, Nussbaumer *et al.*, [8] investigated the effect of co-combustion, revealing that sulfur dioxide emissions decreased when the ratio of biomass increased due to the small amount of sulfur element in the biomass. In addition, the effect of co-firing biomass on furnace efficiency was investigated by Wang *et al.,* [9]. The increase in biomass co-firing level resulted in a decrease in furnace efficiency, as the content of unburned carbon rose after combustion.

Computational fluid dynamics (CFD) is a numerical calculation method employed to study fluid behavior with considerations for momentum, energy, and mass conservation. This widely used simulation method spans various disciplines such as chemical engineering, mechanical engineering, and biomedical engineering [10]. Notably, prior studies on CFD simulation of combustion models often overlooked the devolatilized reaction of solid fuel [11,12]. If the devolatilized reaction of solid fuel is included, it will affect the volatile gases that release from the solid fuel. Then, the effect of the devolatilized reaction makes the model realistic.

Given these considerations, this study investigates the fuel feeding ratio in co-firing power plants using computational fluid dynamics to assess its impact on boiler operating conditions. Optimization of flue gas emissions post-combustion is also a critical aspect. The study's challenge lies in simulating fuel as a solid phase and incorporating the devolatilization reaction to govern this phenomenon.

## 2. Governing Equation

The system of the boiler that is considered in this study is the fluidized bed with combustion chemical reactions. Here, the two-fluid model, or Eulerian-Eulerian, together with kinetic theory of granular flow is used for the simulation of fluidized beds which successfully used in several studies [5,13]. The momentum conservation, energy conservation, and mass conservation for a multiphase system with species transport are shown in the equation (1)-(7) [14] in Table 1. The conservation equations (equations (1) – (4)) contain the accumulation term for solving the dynamic behaviour, the diffusion and convection terms for addressing spatial problems, and the source term or additional sources of force, energy, and mass for momentum, energy, and species transport, respectively.

**Table 1**
Governing equation for co-firing boiler combustion CFD simulation

| | Description | Equation |
|---|---|---|
| (1) | Mass conservation | $\frac{\partial}{\partial t}(\alpha_q \rho_q) + \nabla \cdot (\alpha_q \rho_q \vec{v}_q) = 0$ |
| (2) | Species conservation | $\frac{\partial}{\partial t}(\rho^q \alpha^q Y_i^q) + \nabla \cdot (\rho^q \alpha^q \vec{v}^q Y_i^q) = \alpha^q R_i^q + \mathcal{R}$ |
| (3) | Energy conservation | $\frac{\partial}{\partial t}(\alpha_q \rho_q h_q) + \nabla \cdot (\alpha_q \rho_q \vec{v}_q h_q) = \alpha_q \frac{\partial p_q}{\partial t} + \bar{\bar{\tau}}_q : \nabla \vec{v}_q - \nabla \cdot \vec{q}_q$ |
| (4) | Momentum conservation | $\frac{\partial}{\partial t}(\alpha_q \rho_q \vec{v}_q) + \nabla \cdot (\alpha_q \rho_q \vec{v}_q \vec{v}_q) = -\alpha_q \nabla p + \nabla \cdot \bar{\bar{\tau}}_q + \alpha_q \rho_q \vec{g} + K_{pq}(\vec{v}_q - \vec{v}_p)$ |
| (5) | Gidaspow drag model | $K_{pq} = \begin{cases} \frac{3}{4} C_D \frac{\alpha_p \alpha_q \rho_q \lvert \vec{v}_p - \vec{v}_q \rvert}{d_p} \alpha_q^{-2.65} & ; \alpha_q > 0.8 \\ 150 \frac{\alpha_p (1-\alpha_q) \mu_q}{\alpha_q d_p^2} + 1.75 \frac{\rho_q \alpha_p \lvert \vec{v}_p - \vec{v}_q \rvert}{d_p} & ; \alpha_q \leq 0.8 \end{cases}$ |
| (6) | Drag coefficient | $C_D = \frac{24}{\alpha_q Re_p}\left(1 + 0.15(\alpha_q Re_p)^{0.687}\right)$ |
| (7) | Gunn interphase heat transfer model | $Nu_p = (7 - 10\alpha_q + 5\alpha_q)\left(1 + 0.7 Re_p^{0.2} Pr^{\frac{1}{3}}\right) + (1.33 - 2.4\alpha_q + 1.2\alpha_q^2) Re_p^{0.7} Pr^{\frac{1}{3}}$ |

| | | | | | |
|---|---|---|---|---|---|
| $\alpha_q$ | Volume fraction for phase q | (-) | $\vec{q}_q$ | heat flux | (W/m$^2$) |
| $\rho_q$ | Density for phase q | (kg/m$^3$) | $\vec{g}$ | Gravitational acceleration | (m/s$^2$) |
| $\vec{v}_q$ | Velocity for phase q | (m/s) | $K_{pq}$ | Drag force | (N) |
| $Y_i^q$ | Mass fraction of species i for phase q | (-) | $d_p$ | Diameter of solid | (m) |
| $R_i^q$ | Rate of reaction of species i for phase q | (kmol/m$^3$s) | $C_D$ | Drag coefficient | (-) |
| $\mathcal{R}$ | Rate of heterogeneous reaction | (kmol/m$^3$s) | $Re_p$ | Reynolds number | (-) |
| $p_q$ | Pressure for phase q | (Pa) | $Nu_p$ | Nusselt number for phase q | (-) |
| $\bar{\bar{\tau}}_q$ | Shear-stress tensor | (Pa) | $Pr$ | Prandtl number | (-) |

The finite volume numerical method is used for solving differential equations by using commercial software, ANSYS Fluent 2023 R1, as a CFD solver. For species transport, the kinetic reaction for fuel combustion is based on the Arrhenius equation that is followed by Xie *et al*., [13]. In this study, 9 chemical reactions are employed, which are shown in Table 2. R1, R2, and R5 are heterogeneous reactions for coal and biomass devolatilization, and char combustion, respectively. The rest of the reaction is oxidation in the gas phase, which was obtained from Xie *et al*., and Miltner *et al*., [4,15].

**Table 2**
Chemical reaction in this study

| | Reaction equation | Rate of reaction | Kinetics constant |
|---|---|---|---|
| R1 | $\text{Woodchip} \rightarrow \text{C} + \text{CH}_4 + \text{H}_2 + \text{CO}_2 + \text{CO} + \text{HCN} + \text{H}_2\text{S} + \text{HCl} + \text{ASH}$ | $r_1 = k_1 C_{Volatile}$ | $k_1 = 1.901 \times 10^4 \exp\left(-\frac{5.882\times10^7}{RT}\right)$ |
| R2 | $\text{Coal} \rightarrow \text{C} + \text{CH}_4 + \text{H}_2 + \text{CO}_2 + \text{CO} + \text{HCN} + \text{H}_2\text{S} + \text{ASH}$ | $r_2 = k_2 C_{Volatile}$ | $k_2 = 8.276 \times 10^4 \exp\left(-\frac{7.3\times10^7}{RT}\right)$ |
| R3 | $\text{H}_2 + 0.5\text{O}_2 \rightarrow \text{H}_2\text{O}$ | $r_3 = k_3 C_{O_2} C_{H_2}^{1.5}$ | $k_3 = 5.159 \times 10^{15} \exp\left(-\frac{28517}{RT}\right) T^{-1.5}$ |
| R4 | $\text{CH}_4 + 2\text{O}_2 \rightarrow \text{CO}_2 + 2\text{H}_2\text{O}$ | $r_4 = k_4 C_{CH_4} C_{O_2}$ | $k_4 = 3.552 \times 10^{14} \exp\left(-\frac{130530}{RT}\right) T^{-1}$ |
| R5 | $\text{C} + \text{O}_2 \rightarrow \text{CO}_2$ | $r_5 = k_5 C_C C_{O_2}$ | $k_5 = 0.002 \exp\left(-\frac{7.9 \times 10^7}{RT}\right)$ |
| R6 | $\text{CO} + 0.5\text{O}_2 \rightarrow \text{CO}_2$ | $r_6 = k_6 C_{CO} C_{O_2}^{0.5}$ | $k_6 = 1.0 \times 10^{15} \exp\left(-\frac{133024}{RT}\right)$ |
| R7 | $\text{H}_2\text{S} + 1.5\text{O}_2 \rightarrow \text{SO}_2 + \text{H}_2\text{O}$ | $r_7 = k_7 C_{H_2S} C_{O_2}$ | $k_7 = 5.2 \times 10^8 \exp\left(-\frac{19300}{RT}\right)$ |
| R8 | $\text{HCN} + \text{O}_2 \rightarrow \text{NO} + \text{CO} + 0.5\text{H}_2$ | $r_8 = k_8 C_{HCN} C_{O_2}$ | $k_8 = 1.0 \times 10^{10} \exp\left(-\frac{280282}{RT}\right)$ |
| R9 | $\text{HCN} + \text{NO} \rightarrow \text{N}_2 + \text{CO} + 0.5\text{H}_2$ | $r_9 = k_9 C_{HCN} C_{NO}$ | $k_9 = 3.0 \times 10^{12} \exp\left(-\frac{250983}{RT}\right)$ |

## 3. Methodology

### *3.1 Computational Domain Construction*

The co-firing power plant in the riser part of the boiler is investigated in this study, which is based on the industrial power plant as shown in Figure 1. The boiler contains three main parts: the fuel and air feeding zone at the bottom of the chamber, the heat exchanger zone at the middle of the chamber height, and the 4 of flue gas outlet at the top of the chamber. For fuel and air feeding zones, there are 6 inlets of fuel feeding, 16 inlets of primary air (PA) at the lower level, 10 inlets of secondary air (SA) at the lower level, 10 inlets of SA at the upper level, and 2 inlet of ash recirculation. In the case of the heat exchanger zone, there are two parts of the heat exchanger: the reheater and the superheater for steam production by heat transfer. The reheater contains 20 racks of steam pipe, and the superheater contains 40 racks of steam pipe.

This 3-dimensional computational domain is constructed by ANSYS design modeler 2023 R1. The fuel and air are fed at the bottom of the chamber; the operating conditions of the air and fuel and the properties of the solid phase are shown in Table 3. According to the circulating fluidized bed operation of this boiler, the bed is sand with 65 tons in the chamber at the initial stage of operation. After the geometry construction, this model has been discretized for numerical calculation by ANSYS meshing with a tetrahedral grid. The authors have separated the number of grid elements into 3 cases: fine grid, medium grid, and coarse grid, for the grid-independent test. The grid-independency test is an evaluation to find the optimal grid element that is appropriate for model calculation and to obtain the accuracy of the solution with the minimum resource of processor calculations.

The assumptions of this study are that the devolatilization of coal and woodchip follows R1 and R2, the unburned solid is treated as the ASH component, and the char component is treated as solid carbon. Additionally, NO emission is considered as the $NO_x$ component, and $SO_2$ emission is considered as the $SO_x$ component.

**Table 3**
Operating condition of air, solid fuel, and sand

| Condition | Value | Unit | Condition | Value | Unit |
|---|---|---|---|---|---|
| Primary air at bottom | 68.09 | $Nm^3/s$ | Solid fuel mass flowrate | 4.02 | kg/s |
| Primary air lower level | 18.24 | $Nm^3/s$ | Woodchip to coal ratio | 0.486 | - |
| Secondary air lower level | 18.21 | $Nm^3/s$ | Solid fuel average diameter | 0.014 | m |
| Secondary air upper level | 16.37 | $Nm^3/s$ | Woodchip density | 413 | $kg/m^3$ |
| Primary air temperature | 479 | K | Coal density | 1,019 | $kg/m^3$ |
| Secondary air temperature | 492 | K | Sand average diameter | 139 | µm |
| | | | Sand density | 2,650 | $kg/m^3$ |

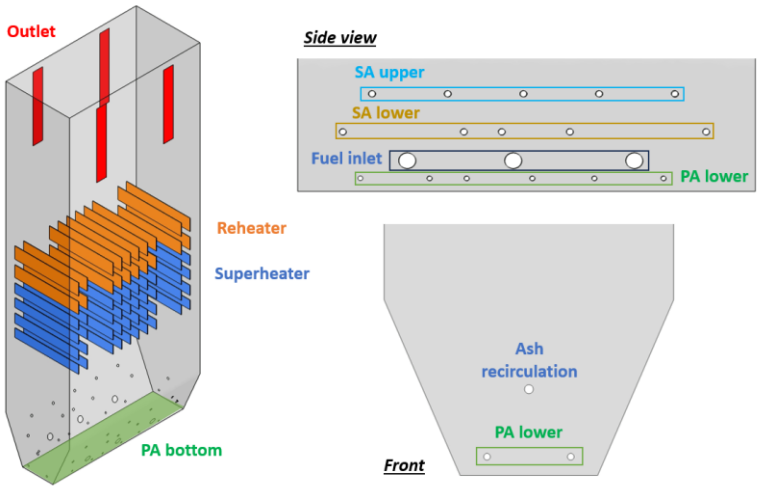


**Fig. 1.** The overview of boiler configuration in oblique-view, side-view, and front-view of boiler

### *3.2 Simulation Setup*

The model of a co-firing boiler contains three phases: the gas phase as a primary or continuous phase, the sand phase as an inert phase, and the solid phase as a solid fuel to represent the woodchip, coal, char, and ash components. The gas phase consists of 12 components of gas species: carbon dioxide ($CO_2$), water ($H_2O$), oxygen ($O_2$), methane ($CH_4$), hydrogen ($H_2$), carbon monoxide (CO), hydrogen sulfide ($H_2S$), sulfur dioxide ($SO_2$), hydrogen chloride (HCl), nitrogen oxide (NO), hydrogen cyanide (HCN), and nitrogen ($N_2$). The properties of gas, for example, density, viscosity and enthalpy of formation are based on the ANSYS Fluent 2023 R1 database [14]. According to the Reynolds number calculation, the value of 85,000 is in the turbulent regime [16]. In this study, the k-ε turbulence model is then used to simulate the fluctuation of the fluid. This model is calculated based on transport equation for turbulence kinetic energy (k) and turbulence dissipation (ε). This model is economy and reasonable for wide range of turbulent flows explain its popularity in industrial flow and heat transfer simulation [14].

For the boundary conditions, the fuel inlet is set as mass flow rate boundary conditions, and the air inlet, both primary and secondary air, is set as velocity inlet boundary conditions, based on Table 3. In addition, the outlet of flue gas is set as pressure outlet boundary conditions with a value of -0.26 kPa obtained from the operating data. The wall of the riser part is treated with a no-slip wall boundary condition, which sets the velocity at the wall surface to zero. In the model, there are 2 zones of heat exchangers: the reheater and the superheater, both set into the convection heat transfer of the wall boundary condition.

For the multiphase interaction, the drag model used in this study is the Gidaspow drag model, as shown in equation (5), combines Wen and Yu for the dilute phase behavior and the Ergun drag model for the dense phase behaviour [14]. The heat transfer between the granular and gas phases is calculated using the Gunn model, as shown in the equation (7), to determine the Nusselt number for interphase heat transfer between gas-solid fuel and gas-sand [17].

## 4. Results and Discussion

### *4.1 Grid Independency Test*

From the grid construction, there are 3 element numbers and their statistical parameters which are in the criteria of recommendation for CFD simulation [18], as shown in Table 4. The aspect ratio represents the relationship between the longest and shortest lengths, while skewness denotes the ratio of deviation between the ideal and actual cell. Furthermore, it is advised to use an aspect ratio of 10 and a skewness of 0.25 for CFD simulation, with the selected element sizes falling within this specified range. Here, both the aspect ratio and skewness values are according to the appropriate values. Besides, the grid-independency test is conducted with the air flow in the riser case using a constant velocity magnitude of 2.5 m/s. From the result in Figure 2 which shows the averaged velocity magnitude in gas phase at the outlet window, 0.4 m of element size is used for further simulation. According to this element size, it can calculate the obtained velocity value as close as the fine grid, 0.3 m of element size. In addition, the cross-sectional view of grid element in each case is shown in Figure 3. The number of elements in the red circle increased when the element size decreased, as the fineness of grid elements can predict the accuracy of simulation results.

**Table 4**
Statistical parameters for each grid element size

| Element size (m) | Aspect ratio average | Skewness average | Element number |
|---|---|---|---|
| 0.5 (coarse) | 1.998 | 0.252 | 577,485 |
| 0.4 (medium) | 1.947 | 0.244 | 715,381 |
| 0.3 (fine) | 1.909 | 0.236 | 1,065,875 |

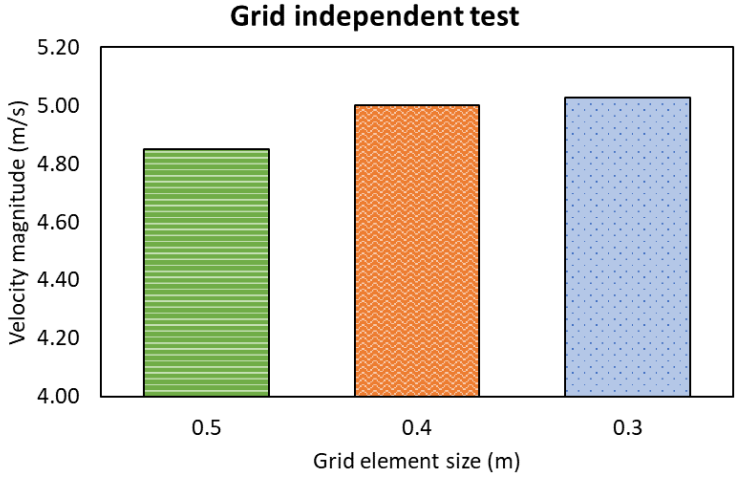


**Fig. 2.** Velocity magnitude at the outlet window for each grid element size

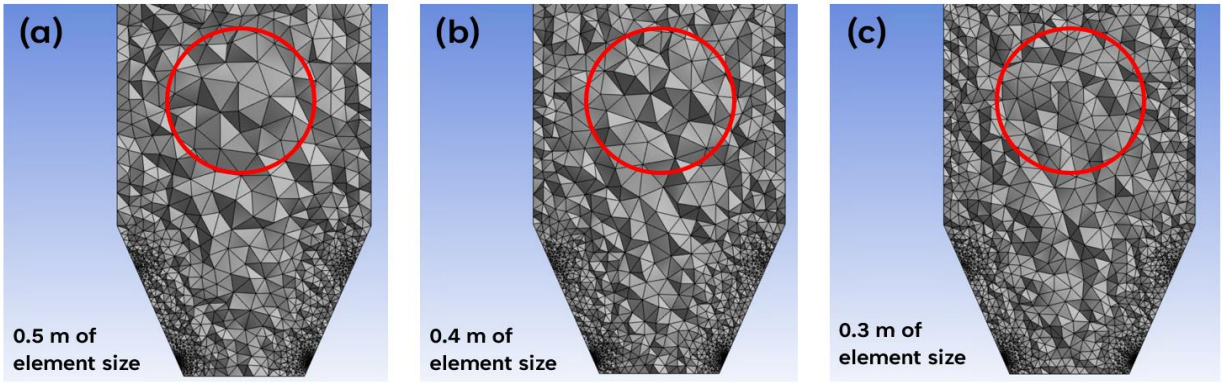


**Fig. 3.** The number of grid element following by the element size for (a) 0.5 m, (b) 0.4 m, and (c) 0.3 m

### *4.2 Model Validation*

The model is validated with the operating data of industrial power plant. From Figure 4, the results of $CO_2$ concentration and flue gas temperature over time indicate that this system reached a steady state at 50 seconds. The results are shown in Figure 5. Flue gas velocity, $CO_2$ percentage by weight, bed temperature, and flue gas temperature are selected for model validation, The velocity of flue gas, amount of $CO_2$, and flue gas temperature are measured by using a probe at the outlet, and the bed temperature is measured at the temperature probe at the bed level. From Figure 5, the model validation result has a small relative error between the operating data and simulation results, with the error of 6.8%, 2.7%, 9.1%, and 3.6% for flue gas velocity, carbon dioxide percentages, bed temperature, and flue gas temperature, respectively.

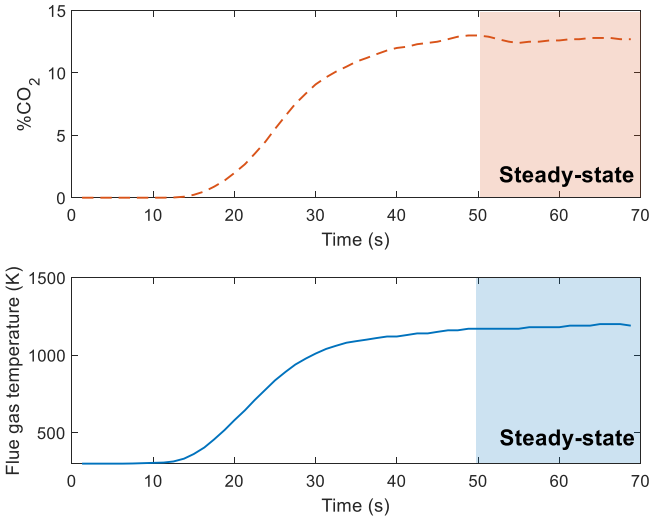


**Fig. 4.** The time independence test of carbon dioxide percentages and flue gas temperature

Figure 6 displays the contour of flue gas velocity, mass fraction of $CO_2$, and gas temperature. Observably, the flue gas velocity is higher at the inlet air and subsequently diminishes with the boiler reactor height. The concentration of $CO_2$ is dense at the bottom due to the devolatilization of solid fuel around the inlet fuel and the oxidation reaction of the volatile component. As the height of the boiler increases, the $CO_2$ concentration decreases due to occurring side reactions, expanding the volume of the reactor by 40%, thereby slightly diluting the $CO_2$ concentration. Regarding the

temperature contour, it illustrates the impact of the heat exchanger, wherein the energy of the flue gas is transferred into water, resulting in a reduction of gas temperature within the heat exchanger zone.

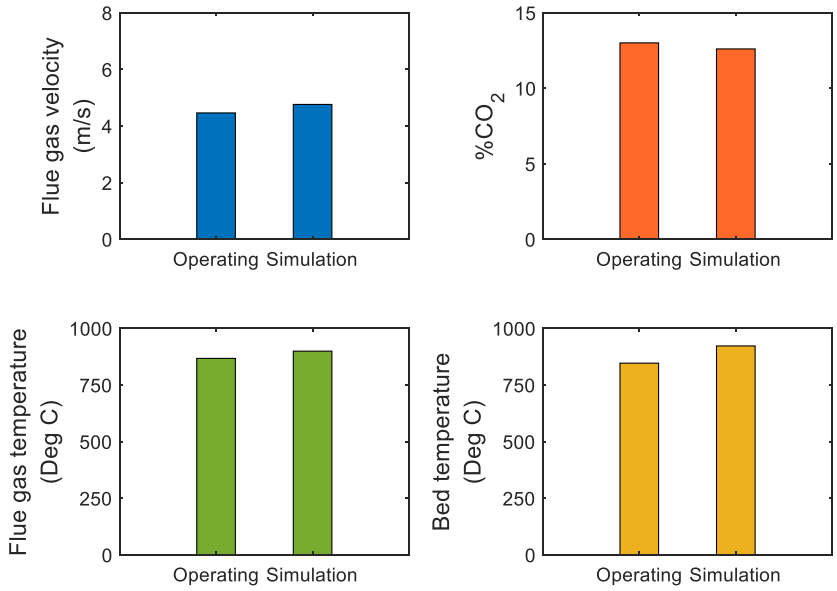


**Fig. 5.** Validation results with industrial power plant data: Flue gas velocity, %$CO_2$, Flue gas and bed temperature

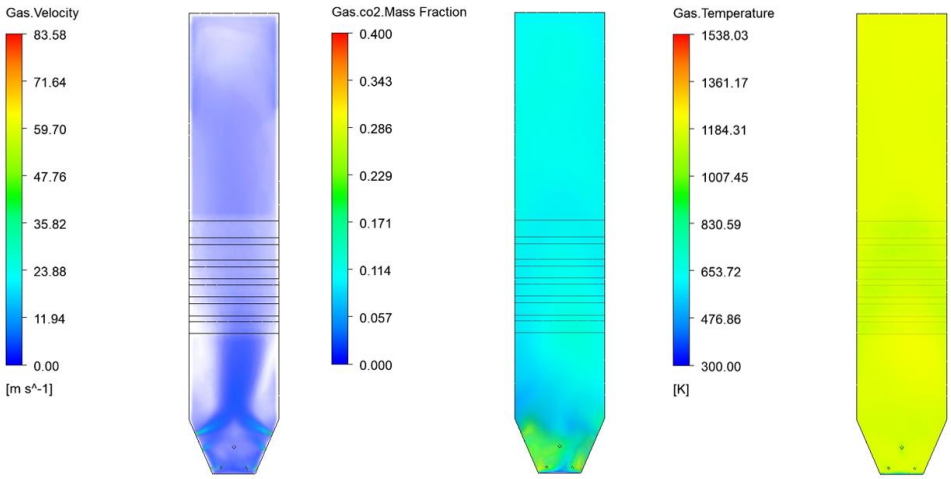


**Fig. 6.** Contour results of gas velocity, $CO_2$ mass fraction, and gas temperature

### *4.3 Effect of biomass to coal feeding ratio*

Variation of biomass fuel feeding ratio from 33% to 86.6% by weight is investigated based on records of real operating data. The results are shown in Figure 7. When the woodchip percentage increasing, the amount of $CO_2$ decreased due to the effect of volatile combustion [7], and the amount of volatile components in biomass structure was higher than coal [6]. The amount of $SO_x$ has in the same trend as the amount of $CO_2$ because the sulfur component in the woodchip is lower than coal. For this reason, the $SO_x$ emission, that came from oxidation reaction of hydrogen sulfide, in the high blending biomass feeding ratio is also small. In contrast, the amount of $NO_x$ emissions is increasing

while the ratio of woodchips in the fuel feed is increasing. This is because the higher ratio of coal contains a higher amount of carbon element that affects the amount of $O_2$ for the oxidation reaction [4]. $NO_x$ formation, that came from the oxidation reaction of hydrogen cyanide, is decreasing as more $O_2$ is consumed in $CO_2$ formation. So that, the $NO_x$ is slightly increasing when the woodchip ratio of fuel feeding increased.

For the boiler efficiency $(\eta)$, which is calculated following by equation (8), where $Q_{loss,FG}$ is the heat loss with flue gas (J/s), $m_{FG}$ is flue gas mass flowrate (kg/s), $h_{FG}$ is mass enthalpy of flue gas (J/kg), $m_{fuel}$ is fuel mass flowrate (kg/s), and $H_{fuel}$ is heating value of solid fuel (J/kg). If the ratio of biomass increases, the boiler efficiency trend decreases due to the total heating value of co-firing solid fuel. The heating value of woodchip and coal are equal to 2,075 kcal/kg, and 4,681 kcal/kg respectively. If the woodchip blending ratio increased, the heating value of solid fuel decreased.

$$\eta = 1 - \frac{Q_{loss,FG}}{m_{fuel}H_{fuel}} = 1 - \frac{\Delta(m_{FG}h_{FG})}{m_{fuel}H_{fuel}} \tag{8}$$

For the optimized operating condition, the objective function is set to minimize the pollution emission, $NO_x$ should be lower than 150 ppm and $SO_x$ should be lower than 200 ppm, based on Scala *et al.*, [19], and to maximize boiler efficiency within the range of 33% to 86.6% of woodchip fuel feeding. The result found that the optimized woodchip percentage is 59.15%, which produces $NO_x$ and $SO_x$ at 123 ppm and 200 ppm, respectively, and the boiler efficiency is 82.84%. The simulated boiler efficiency is relevant to the typical coal and biomass feed boiler [20].

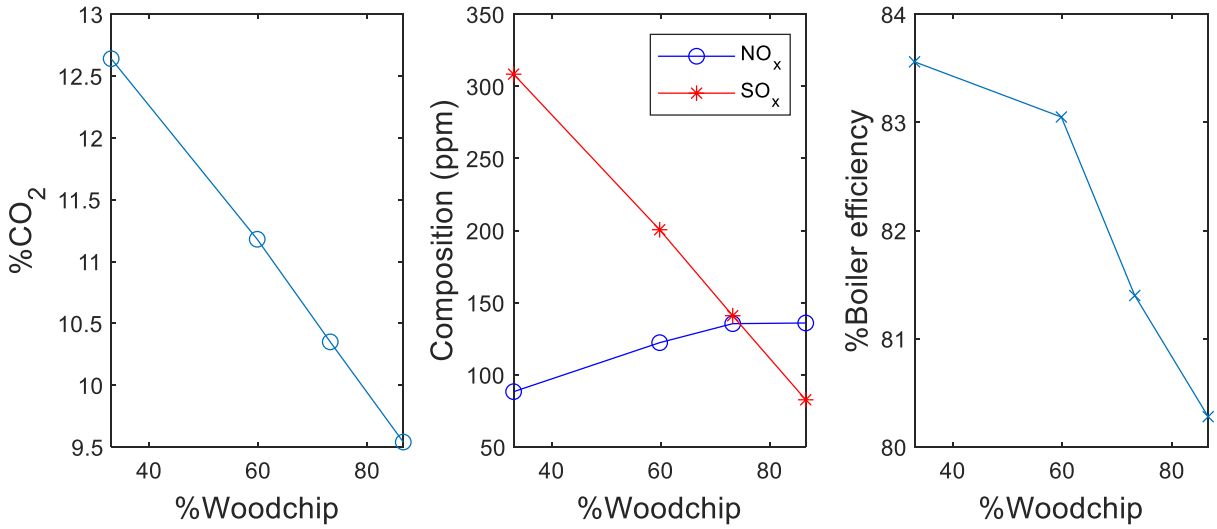


**Fig. 7.** Effect of %Woodchip to $\%CO_2$, composition of $NO_x$ and $SO_x$, and boiler efficiency

## 5. Conclusion

Currently, global energy consumption has experienced a significant increase, and biomass stands out as a preferable option for renewable energy. Electricity, a crucial form of energy, can be generated from power plants. Typically, coal serves as the primary fuel in boiler feed, but considering pollution concerns, biomass is introduced to create a blended fuel ratio with coal. Consequently, the impact of the biomass fuel feeding ratio is scrutinized through computational fluid dynamics simulation. The domain construction is three-dimensional, and it has been discretized with an appropriate number of grid elements. Subsequently, the model undergoes validation using operating

data, revealing minimal errors. Regarding the effect of biomass blending ratios, an increase in the woodchip ratio in the feed results in a decrease in sulfur oxide emissions, attributed to coal being the primary sulfur source. However, this change leads to a decline in boiler efficiency due to the reduced heating value of the fuel mixture. Finally, the optimized woodchip ratio is determined to be 59.15%, with nitrogen oxide and sulfur oxide emissions at 123 and 200 ppm, respectively, and a boiler efficiency of 82.84%. Still, the limitations of this study are the uniform size of solid fuel, and the variation of solid fuel and air flowrate are neglected and keep constant in this study.

**Acknowledgement**
This study is financial supported by the Program Management Unit for Competitiveness (PMU-C), Office of National Higher Education Science Research and Innovation Policy Council, Thailand (No. C10F650236). In addition, the co-funding from Integrated Research Center (IRC), Thailand and the facility from Chulalongkorn University is acknowledged. In addition, the National Research Council of Thailand / Chulalongkorn University for providing the Mid-Career Research Grant (N42A660438) is acknowledged.

**References**

[1] *Energy consumption by source*. 2022.
[2] Yanguo Zhang, Qinghai Li, and Hui Zhou, *Chapter 4 - Heat Transfer in Fluidized Beds*, in *Theory and Calculation of Heat Transfer in Furnaces*, Y. Zhang, Q. Li, and H. Zhou, Editors. 2016, Academic Press: Oxford. p. 101-129. https://doi.org/10.1016/B978-0-12-800966-6.00004-1
[3] J. Adánez, P. Gayán, L. F. de Diego, F. García-Labiano, and A. Abad. "Combustion of Wood Chips in a CFBC. Modeling and Validation." *Industrial & Engineering Chemistry Research* 42, no. 5 (2003): 987-999. https://doi.org/10.1021/ie020605z
[4] Jun Xie, Wenqi Zhong, Yingjuan Shao, Qian Liu, Longhai Liu, and Guoyao Liu. "Simulation of Combustion of Municipal Solid Waste and Coal in an Industrial-Scale Circulating Fluidized Bed Boiler." *Energy & Fuels* 31, no. 12 (2017): 14248-14261. https://doi.org/10.1021/acs.energyfuels.7b02693
[5] Blaid Alganash, Manosh C. Paul, and Ian A. Watson. "Numerical investigation of the heterogeneous combustion processes of solid fuels." *Fuel* 141 (2015): 236-249. https://doi.org/10.1016/j.fuel.2014.10.060.
[6] Stanislav V. Vassilev, David Baxter, Lars K. Andersen, and Christina G. Vassileva. "An overview of the chemical composition of biomass." *Fuel* 89, no. 5 (2010): 913-933. https://doi.org/10.1016/j.fuel.2009.10.022
[7] Gyeong-Min Kim, Jae Hyung Choi, Chung-Hwan Jeon, and Dong-Ha Lim. "Effects of Cofiring Coal and Biomass Fuel on the Pulverized Coal Injection Combustion Zone in Blast Furnaces." *Energies* 15, no. 2 (2022): 655. https://doi.org/10.3390/en15020655
[8] Thomas Nussbaumer. "Combustion and Co-combustion of Biomass: Fundamentals, Technologies, and Primary Measures for Emission Reduction." *Energy & Fuels* 17, no. 6 (2003): 1510-1521. https://doi.org/10.1021/ef030031q
[9] Xuebin Wang, Zia Ur Rahman, Zhaomin Lv, Yiming Zhu, Renhui Ruan, Shuanghui Deng, Lan Zhang, and Houzhang Tan. "Experimental Study and Design of Biomass Co-Firing in a Full-Scale Coal-Fired Furnace with Storage Pulverizing System." *Agronomy* 11, no. 4 (2021): 810. https://doi.org/10.3390/agronomy11040810
[10] Jiyuan Tu, Guan-Heng Yeoh, and Chaoqun Liu, *Chapter 1 - Introduction*, in *Computational Fluid Dynamics (Third Edition)*, J. Tu, G.-H. Yeoh, and C. Liu, Editors. 2018, Butterworth-Heinemann. p. 1-31. https://doi.org/10.1016/B978-0-08-101127-0.00001-5
[11] Wenchao Ma, Xu Liu, Chen Ma, Tianbao Gu, and Guanyi Chen. "BASIC: A Comprehensive Model for SOx Formation Mechanism and Optimization in Municipal Solid Waste (MSW) Combustion." *ACS Omega* 7, no. 5 (2022): 3860-3871. https://doi.org/10.1021/acsomega.0c03287
[12] Mohammadreza FarokhiMadjid Birouk. "Application of Eddy Dissipation Concept for Modeling Biomass Combustion, Part 2: Gas-Phase Combustion Modeling of a Small-Scale Fixed Bed Furnace." *Energy & Fuels* 30, no. 12 (2016): 10800-10808. https://doi.org/10.1021/acs.energyfuels.6b01948
[13] Jun Xie. "Three-Dimensional Eulerian–Eulerian Modeling of Gaseous Pollutant Emissions from Circulating Fluidized-Bed Combustors." *Energy & Fuels* v. 28, no. no. 8 (2014): pp. 5523-5533-2014 v.28 no.8. https://doi.org/10.1021/ef501095r
[14] ANSYS, *ANSYS Fluent theory guide*. 2013.

[15] Martin Miltner, Aleksander Makaruk, Michael Harasek, and Anton Friedl. "Computational fluid dynamic simulation of a solid biomass combustor: modelling approaches." *Clean Technologies and Environmental Policy* 10, no. 2 (2008): 165-174. https://doi.org/10.1007/s10098-007-0137-0

[16] E. Shashi Menon, *Chapter Five - Fluid Flow in Pipes*, in *Transmission Pipeline Calculations and Simulations Manual*, E. Shashi Menon, Editor. 2015, Gulf Professional Publishing: Boston. p. 149-234. https://doi.org/10.1016/B978-1-85617-830-3.00005-5

[17] B. Sun, S. Tenneti, and S. Subramaniam. "Modeling average gas–solid heat transfer using particle-resolved direct numerical simulation." *International Journal of Heat and Mass Transfer* 86 (2015): 898-913. https://doi.org/10.1016/j.ijheatmasstransfer.2015.03.046.

[18] Simscale. *Mesh Quality*. 2023.

[19] Fabrizio Scala, Amedeo Lancia, Roberto Nigro, and Gennaro Volpicelli. "Spray-Dry Desulfurization of Flue Gas from Heavy Oil Combustion." *Journal of the Air & Waste Management Association* 55, no. 1 (2005): 20-29. https://doi.org/10.1080/10473289.2005.10464604

[20] Esa Kari Vakkilainen, *3 - Boiler Processes*, in *Steam Generation from Biomass*, E.K. Vakkilainen, Editor. 2017, Butterworth-Heinemann. p. 57-86. https://doi.org/10.1016/B978-0-12-804389-9.00003-4